1-1-2012

Analysis of Interphase Chromatin Motion in HeLa Cells

Matthew Joel Westacott
University of Denver

ANALYSIS OF INTERPHASE CHROMATIN MOTION IN HELA CELLS

A Thesis

Presented to

the Faculty of Natural Sciences and Mathematics

University of Denver

In Partial Fulfilment

of the Requirements for the Degree

Master of Science

---

by

Matthew J. Westacott

November 2012

Advisor: Dinah Loerke

Author: Matthew J. Westacott
Title: ANALYSIS OF INTERPHASE CHROMATIN MOTION IN HELA CELLS
Advisor: Dinah Loerke
Degree Date: November 2012

Abstract

Motion of particles under influencing forces may be observed under light microscopy techniques. Variations in mobility of particles may give relevant biophysical information. Automated high resolution single particle tracking techniques were used to characterize interphase chromatin mobility in the cell nucleus. Interphase chromatin undergo replication prior to cell division with the assistance of replication proteins (machinery) which modify chromatin mobility. Using dual color imaging of flourescently tagged chromatin and proliferating cell nuclear antigen (PCNA) were followed through interphase. Chromatin motion was modelled as a two dimensional random walk. Reduction in chromatin mobility was observed during S phase was dependent on proximity to the replication machinery. Mobility during G1 and G2 phase is independent of proximity to GFP-PCNA maxima and is higher than during S phase. These results suggest that replication selectively inhibits chromatin mobility. Local proximity to replication machinery however, cannot account for the entire mobility difference. By modelling the mean square displacement as a power law, sub-diffusive behavior was observed in S phase chromatin whereas non S phase exhibited normal diffusional characteristics.

Table of Contents

List of Figures

Chapter One: Introduction

Chromatin: The subunits and replication

Composition of DNA

Chromatin organization in the nucleus contains sets of hierarchy of structures beginning with the basic composition of the nucleic acids as poly-nucleotides [1]. The four monomer bases: Adenine, Guanine, Tyrosine, Cytosine connect to a deoxyrobiose sugar forming a nuceloside. Together with the addition of alternating phosphate and sugar bonds, nucleosides may link and form long chain poly-nucleotides. The asymmetry with the backbone of DNA leads to a naturally polarized state, the phosphate termination end, referred to as the 5', and the sugar termination end referred to as the 3' [2]. When two strands of DNA come together, they align anti-parallel, this will be seen later as a block in the replication process. Tertiary structure was resolved by Watson and Crick, consisting of two sets of long poly-nucleotide chains whereby nucleobases are attached through hydrogen bonding. Two bond pairs exists in DNA, between Guanine and Cytosine forming three intermolecular hydrogen bonds, and between Adenine and Thymine forming two intermolecular hydrogen bonds. DNA may exist in several forms, A-DNA Z-DNA or B-DNA, in which the difference occurs in how quickly strand rises in a helical pattern [3,4]. Consider that for a human cell, the length of DNA if stretched from end to end would be approximately 3.0 meters [5].

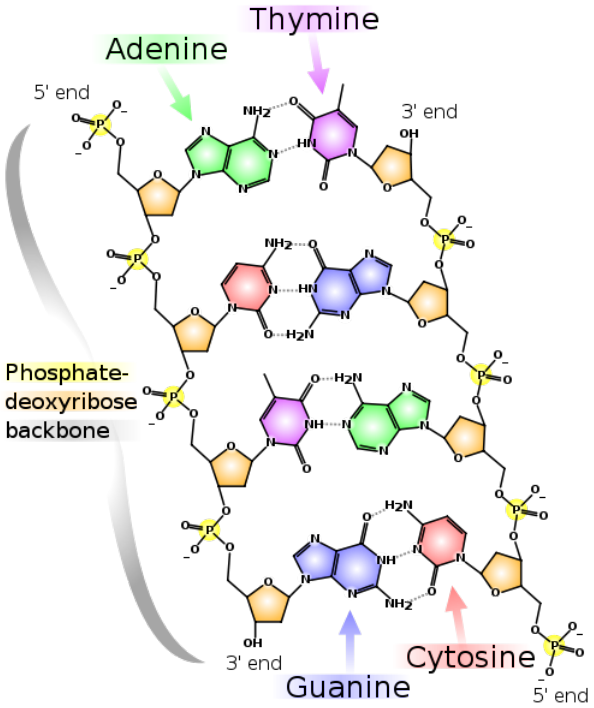

Figure 1: Composition of DNA
Chains of sugar-phosphate bonded nucleotides align anti-parallel and are held by hydrogen bonding between the nucleobases [6].

As such, assembling higher order structures which compact the DNA is a biological necessity. These order structures of DNA assembles in the fundamental unit of the nucleosome, which gives order to an otherwise mass assembly of DNA strands. Electron micrograph images in the showed DNA tethered to chromatin proteins to form a picture described appropriately as ”beads on a string” [7].

Chromatin

The structure of the nucleosome core particle (NCP) was first proposed in 1974, describing it as a repeating complex of eight histone proteins connect by 200 base pairs of DNA [8]. In conjunction with higher resolution electron microscopy and X ray diffraction an appropriate model was constructed giving the NCP a wedge-like shape, whose contents included a set of four histone proteins H2A, H2B, H3 and H4 [9–11].

The ensemble of proteins, or octomer, contains three functional domains including N terminus domains of each protein extended beyond the core. DNA consisting of 146 base pairs is wrapped 1.75 turns around the octomer using several forms of binding processes, primarily through Arginine side chains inserted into the DNA minor grooves which provides induced dipoles with the phosphate backbone of DNA [12]. NCPs are linked together through 30-80 base pairs of linker DNA, and attached through a fourth histone protein H1 this level of structure is commonly referred to as the chromatasome. Higher ordered structure of chromatin is assembled through compaction of the NCPs by first coiling into a "molten mass" with a diameter of 30 nm followed by cohesion proteins to form greater compacted structures however, repetitious structure has yet to be resolved until chromatin has reached metaphase chromosomes [13]. The compaction process continues, until the largest structure of DNA has been compressed up to 400,000 of it's extended length [2, 14] .

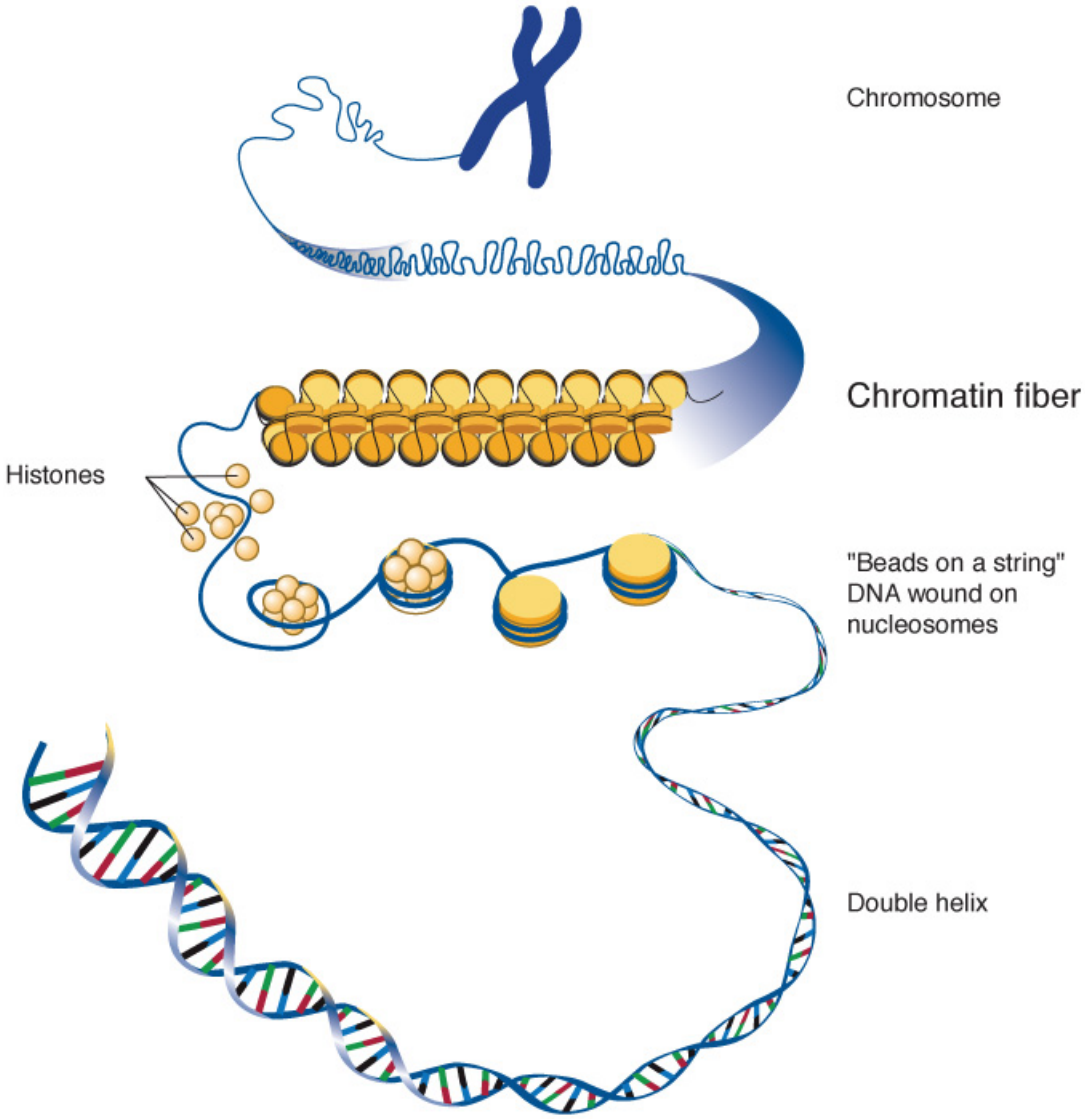

Figure 2: Hierarchy of stucture from DNA to the chromsome.
DNA wrapped around histone core constitutes the primary structure of chromatin.
Higher order structures beyond this have not been resolved and thought to be random.
Consistent structure is resolved in metaphase chromosomes on lengthscales of microns [15].

Two forms of chromatin occupy the nucleus. The initial definition of heterochromatin was first that it stained more intensely which indicated a higher packing ratio, as well as occupying space near the nuclear periphery. It was only later that differences amongst the two arose. Euchromatin is more loosely packed and is more frequently

under transcription [16].

DNA replication and the Cell Cycle

Replication of DNA is highly conserved process through all eukaryotic cells and variations amongst replication proteins are generally restricted to organisms of considerable difference [17]. The task in replication is to unravel the compact structure of chromatin and transcribe the genome, making as little error as possible. Targeted sights called DNA replication origins, which are scattered along DNA, recruit proteins to form a pre-replication complex [18]. These proteins in turn recruit the replication machinery needed to duplicate DNA. DNA helicase travels up the strand from the replication origin splitting the DNA into two strands, DNA Polymerase acts to transcribe the DNA of each strand. Proliferating cell nuclear antigen (PCNA) which acts as our florescent marker for replication machinery acts a procestivity factor for replication by clamping down DNA polymerase to the DNA. Since a polarization exists inside for each strand, there is a preferential direction that polymerase transcribes, in the 5' to 3' direction. One end, the leading strand, is polarized preferentially such that DNA polymerase can transcribe as the helicase splits the DNA. [19].

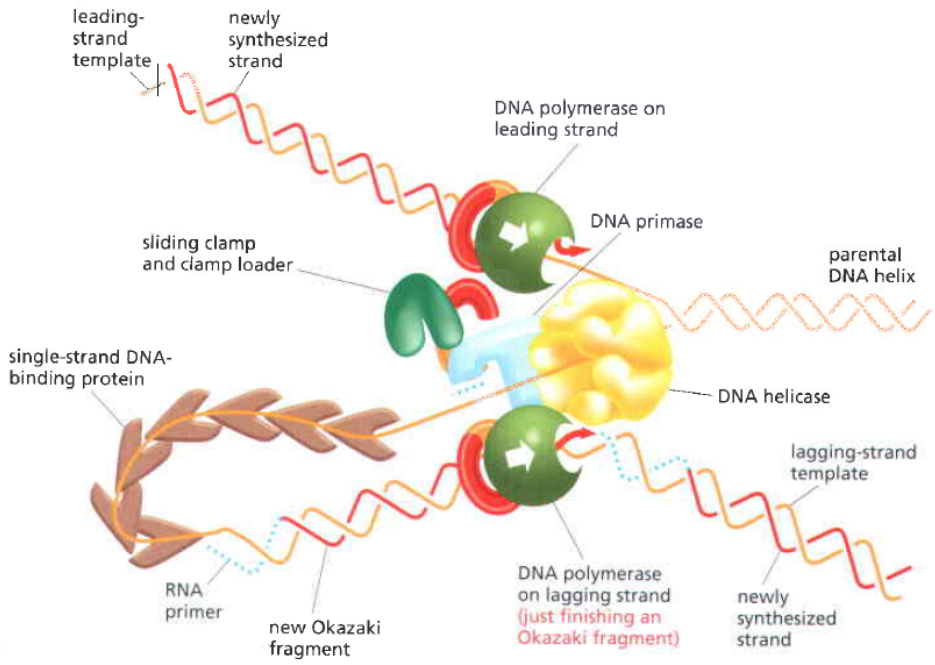

Figure 3: The replication fork
DNA is duplicated with the assistance of replication machinery or accessory proteins DNA is split using DNA helicase to create a replication fork. DNA polyermase acts on both strands in the appropriate manner; by traversing simultaeously thorugh the 5' to 3' leading strand and transcribing in segments on the Okazaki fragment [20] .

The so called lagging strand, the 3' to 5' end, requires the use of RNA polyermase to lay down segments of RNA primer, so called Okazaki fragments which are not yet replicated DNA, but are under hold. DNA polyermase then interchanges the RNA primer with DNA and the process continues. Cells follow a time regimented cycle of replication and division. Each phase of the cell cycle is unique in the abundance of certain proteins which perform the tasks necessary for division. As such, proteins which modify chromatin can be found in each stage of the cell cycle. The parent cell traverses phases G1, S, G2, and the mitosis phases finally before splitting [21].

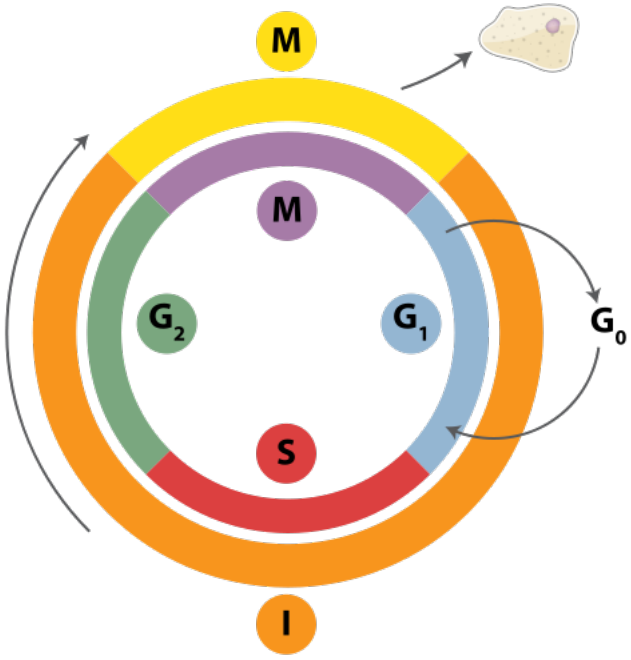

Figure 4: The Cell Cycle
Progression of the cell after division begins in Gap 1 (G1) where the cell begins to increase in size and mass. In synthesis phase (S), DNA is replicated with the use of replication machinery including PCNA and DNA polymerase. The cell in Gap 2 (G2) phase grows and synthesizes proteins required for the two daughter cells [22].

Along with conserving the sequence of nucleic acids, the replication cycle also conserves the histones structure. Through replication the nucleosome must be disassembled by splitting two H2A-H2B dimers and a (H3-H4) tetramer. After the fork has passed the histone complex is assembled through replciation-dependent de novo nucleosome assembly. [23]. Passing of the replication fork allows parental histone (H3-H4) tetramer to redeposit on either strand and *De Novo* histones are deposited onto the strands [24, 25].

The structure of chromatin carries with it epigenetic information that is conserved after replication. Generally, histone modifications act as markers for this information including histone metylation and acetylation. Patterns of modifications contribute to functional chromatin domains and are conserved on each strand after the replication fork [26–28] . The described replication events occur in a subset of interphase, known as S or synthesis phase. Prior to this phase in G1 (or gap 1) phase the nucleus undergoes

the protein creation needed for replication.

Single particle dynamics

Single particle tracking (SPT) has been used in a variety of applications to determine dynamics of a system. The method, rather than bulk experiments, is to observe individual particles with high precision. Biologically, it can be used to observe protein-protein interactions, cellular responses, and membrane structure. [29]. In addition, it contains the potential to observe heterogeneity and sub populations within a system [29, 30] Consider a particle, a protein for example, which is subject to two or more states with a general probability of being in either state. Where as bulk experiments will measure the averaged behavior of all particles, it is possible to observe a particle undergoing transitions between states. The resolution of single particle experiments is often orders of magnitude better than bulk experiments, often with resolutions down to 10-50nm with standard optical light. Although objects under 250nm will create an airy disc and cannot be resolved fully due to the diffraction limit, if the signal to noise ratio is higher than the this resolution limit one can still track displacements of the airy disc down to higher precision. One common form of characterizing the motion of particles is through analysis of the mean square displacement over time. Often, diffusion arises from particle gradients, i.e. distributions of particles spreading from high to low concentration.

If we consider a ensemble of particles in a 1D matrix between with equal probability k of stepping left, right, or staying at center we may write the mean displacement $< \Delta x >$ as

$$< \Delta x >= ak\Delta t + (-a)k\Delta t + 0(1 - 2k\Delta t) = 0 \tag{1}$$

As a particle with equal probability of stepping left or right will not travel any distance, this should be intuitive. The more important parameter is to compute the

mean square displacement

$$< \Delta x^2 >= a^2 k \Delta t + (-a)^2 k \Delta t = 2a^2 k \Delta t \tag{2}$$

Or for perfect diffusion, the square displacement should scale linearly with time.

Brownian Motion and the Langevin Equation

If we start with the unmodified Langevin equation

$$m\frac{dv}{dt} = F + F'(t) - \alpha v \tag{3}$$

Where m is the mass of the particle, v the velocity, F as the external force and it's derivative as thermal fluctuations. If we take the forcing function as 0, and multiply by x to obtain the mean square displacement we find:

$$mx\frac{dv}{dt} = mx\frac{d\dot{x}}{dt} = m\left[\frac{d}{dt}(x\dot{x}) - \dot{x}^2\right] \tag{4}$$

Taking the average of both sides

$$m\left\langle \frac{d}{dt}(x\dot{x}) \right\rangle = m\frac{d}{dt} < x\dot{x} >=< \dot{x}^2 > -\alpha < x\dot{x} > \tag{5}$$

Solving for $< x\dot{x} >$

$$< x\dot{x} >= -\frac{m}{\alpha}\frac{d}{dt} < x\dot{x} > + \frac{1}{\alpha} < \dot{x}^2 > \tag{6}$$

Noting that exponentials would satisfy the derivative we can then write

$$< x\dot{x} >= Ce^{-\gamma t} + \frac{1}{\alpha} < \dot{x}^2 > \tag{7}$$

Taking that all particles start at a position of x=0 at t = 0 we can then solve for C

and re-write as :

$$< x\dot{x} >= \frac{< \dot{x}^2 >}{\alpha}(1 - e^{-\gamma t}) \tag{8}$$

Lastly we can exchange $< x\dot{x} >$ as $\frac{1}{2}\frac{d}{dt} < x^2 >$

$$\frac{1}{2}\frac{d}{dt} < x^2 > \;=\; \frac{< \dot{x}^2 >}{\alpha}(1 - e^{-\gamma t}) \tag{9}$$

$$< x^2 > \;=\; \left(\frac{2 < \dot{x}^2 >}{\alpha}(1 - e^{-\gamma t})\right) dt \tag{10}$$

Performing the integration we find

$$< x^2 >= \frac{2 < \dot{x}^2 >}{\alpha}(t - \gamma^{-1}(1 - e^{-\gamma t})) \tag{11}$$

The finalized mean square displacement of a system. Limiting cases in this expression occur by varying the time around γ. For times much smaller than γ we can taylor expand the second term.

$$< x^2 > \;=\; \frac{2 < \dot{x}^2 >}{\alpha}\left(t - \beta^{-1}(1 - 1 - \beta t + \frac{1}{2}\beta^2 t^2 + ...)\right) \tag{12}$$

$$< x^2 > \;=\; \frac{< \dot{x}^2 > \beta}{\alpha} t^2 \tag{13}$$

This area where the mean square displacement scales as t^2 is more commonly referred to as the ballistic regime. Conceptually it can be understood as the time when a particle is diffusing in a straight line before another particle interaction. The second regime when times are much longer than γ we use the first term in the approximation.

$$< x^2 > \;\; = \;\; \frac{2 < \dot{x}^2 >}{\alpha} t \tag{14}$$

This explains random particle diffusion over long timescales and through interactions with other particles. As our system operates around 1Hz sampling time, this is the only regime where we are able to fully resolve the behavior [31–33].

Chromatin motion in vivo

High-resolution light microscopy techniques with the combination of fluorophores has allowed the viewing of motion of chromatin within the nucleus. The regulation of the chromosome structure in methaphase as well as the confinement of chromatin to nuclear territories and the need for structural changes for DNA transcription all point to a dynamic picture of chromatin within the nucleus [34]. Early studies on chromatin motion in *Drosophila* showed Brownian motion of chromatin with diffusion coefficients of 1x10^{-4} to 1x10^{-3} μm^2/sec. It was also reported that chromatin foci occupied distinct territories of roughly 1 percent of the nuclear volume. Another study with spermatocyte nuclei showed chromatin motion in G1 of 1.3 x10^{-2} μm^2/sec with a confinement radius of 0.3 μm and slower movement over longer timescales with a diffusion coefficient 13 times less than the fast motion and confined to a radius of 0.6 μm. Changes in chromatin motion are correlated with the initiation of replication in S phase and it was proposed that chromatin is tethered to a nuclear matrix [35, 36] .Interestingly, motion in G2 spermocytes showed 4 times slower mobility on shorter timescales. Diffusion of chromatin is typically orders of magnitude slower than protein or even DNA diffusion, and it may be influenced by the compaction of the chromatin fiber, the possible interaction with a nuclear matrix, or interaction with DNA and RNA proteins.

Three distinct modes of motion have been observed within the nucleus [37]. On the shortest time-scales, within a few seconds chromatin undergoes seemingly random

Brownian motion. However, longer range jumps on the order of 150nm and velocities 4 times faster than standard observed diffusion have been observed [38]. Two photon excitation was used with 30ms temporal resolution to monitor chromatin position. These jumps are reduced when ATP is depleted within the nucleus, suggesting they are dependent on an active transport system [39]. Moreover, the recorded diffusion emulates proposed models of active transport, such as the conveyor belt model in which a particle is attached to a moving belt of constant velocity [40] . The next order of motion over the course of minutes over distances of several micrometers are seen to be in response to physiological cues [41, 42]. In CHO cells a VP16 activator was tagged to a segment of the genome on the nuclear periphery and a repositioning to the interior of the nucleus was observed suggesting that transcription and other functions are tied to position [43]. It has been established that euchromatin which occupies the nuclear interior is more often under transcription then its heterochromatin counterpart which is located in the nuclear periphery, and indeed it may appear the position of chromatin is often critical for gene expression [16]. Evidence for chromosome interaction amongst territories is supported by the necessity for transcriptional interaction [44]. Finally, long scale motion of entire genome reorganization during cell division where chromatin rearranges within the nucleus to form the chromosome structure in response to cellular division. In *Drosophila* chromosome domains have been seen transitioning from the nuclear periphery to the interior in response to the cell cycle or changes in transcription behavior [41, 45].

Anomalous Diffusion

Normal Brownian motion in two dimensions can be described in terms of a linear relationship between the mean square displacement and time.

$$< x^2 >= 4Dt \tag{15}$$

If we consider normal scaling to be linear in time, we can describe abnormal or anomalous diffusion as scaling as a power law

$$< x^2 > \propto At^{\gamma} \tag{16}$$

Normal diffusion will satisfy the equation such that $\gamma = 1$. Trajectories with $\gamma > 1$ are classified as super-diffusive and $\gamma < 1$ as sub-diffusive. Causes for such trajectories lie in modifying the behavioral pattern of the particle. Sub-diffusive particles will explore less of their allowed space, typically indicating either binding events to other particles or membranes. The opposite case, in which $\gamma > 1$ will usually indicate an active transport system. When $\gamma = 2$, the case is called ballistic trajectory and the particle is travelling in a ideally straight line. Increasing γ past this indicates accelerating particles, which again would indicate an active transport system. A particle exhibiting either sub or super diffusion does not necessarily indicate anomalous diffusion for the system as a whole. Using the random walk simulation above we may compute mean square displacement of individual trajectories and compute γ values for each. Using particle numbers characteristic of our systems ($\approx$ 1000 with 100 time iterations) we may observe a distribution of γ coefficients for the system that may range between 0.8 and 1.5

If we average together the sum of all trajectories we obtain perfect diffusion. Hence, fluctuations of individual trajectories from the norm is both normal and expected. The average behavior of all trajectories however, should remain within normal diffusion limits unless the system is being modified abnormally. Such modifications often create ergodicity breaking, a concept originated from Boltzmann in his work the ergodic hypothesis.

Ergodicity

If we consider an ensemble of particles with a given set of characteristics the ensemble average of a observable may be written as

$$< f >= \frac{\int_{space} f\rho}{\int_{space} \rho} \tag{17}$$

Were p is the probability density function and f is our observable. For an ensemble of particles, the probability of occupying each state remains constant and each microstate is equally and independent of time hence

$$< f >_{ens} =< f >_{time} \tag{18}$$

Observing each particle for long enough periods should be invariant hence observing the actions of single particles should be the same as observing the average behaviour of all particles. Ergodicity breaking occurs when this postulate is violated, indicating irregular particle behavior [46]. With our observable quantity, the displacement of particles, we may write that the ensemble average of mean square displacements is

$$< R^2 >_{ens} = \frac{1}{N} \sum_{j}^{N} R_{i,j}^2 \tag{19}$$

Where R^2 is the frame to frame displacement at each frame i and for each particle j. We may then write the time average for each particle as

$$< R^2 >_{temp} = \frac{1}{T} \sum_{i}^{T} R_{i,j}^2 \tag{20}$$

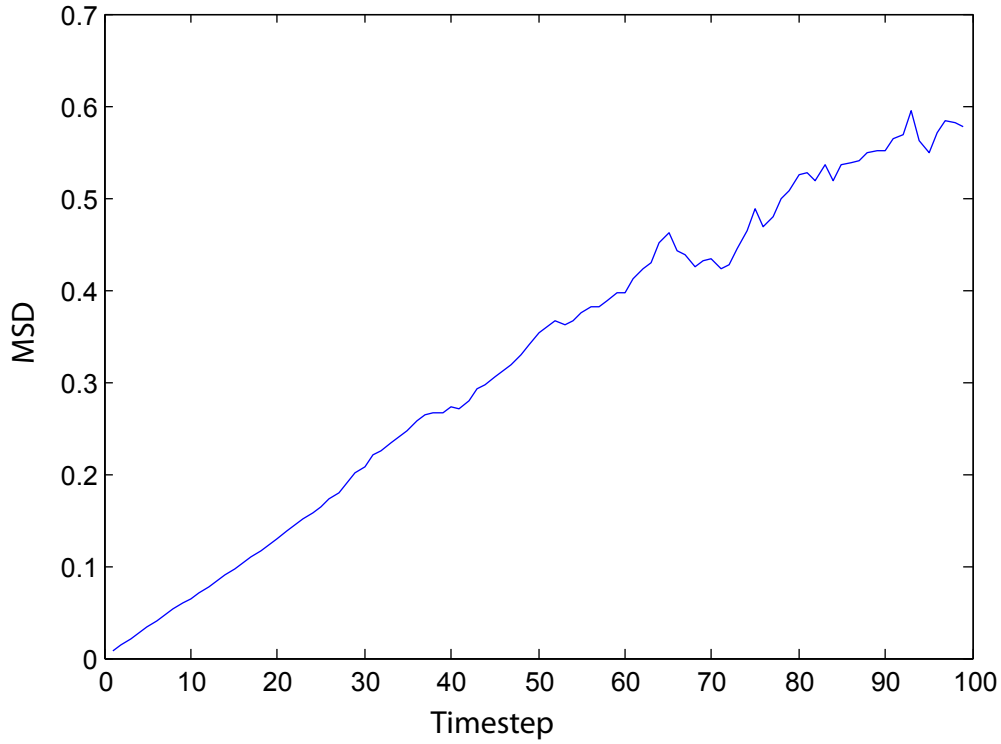

Figure 5: Simulation MSD
Mean square displacement of a simulation using N=2000 and T=100s. Trajectories have a small probability of terminating at each timestep thus behavior over longer periods become noisy.

Random Walk Simulations

Random walk simulations code can be easily implemented in MATLAB and can be used to weigh statistical relevance of parameters on experimental data. In classical 2D Brownian motion a particle can be assigned both a random direction and step size. While the step size can be given any random distribution, (i.e. Poisson, Laplace), a Gaussian distribution of step sizes is empirically seen in the data, so such a model should be used for simulations. The mean square displacement of each particle at time point t can be calculated using the following form:

$$< x^2(t) >= \sum_{i=1}^{t} |\mathbf{r}(\mathbf{t_i}) - \mathbf{r}(\mathbf{t_{i-1}})|^2 \tag{21}$$

While Brownian models describe particle trajectories whose mean square displacement increases linearly in time, the timescales used in simulations ensure particles with behaviors exhibiting both super and sub diffusion processes. To quantify the diffusion characteristic one can approximate the mean square displacement with the following.

$$< x^2 > \approx At^{\gamma} \tag{22}$$

Where γ is the characteristic descriptor of motion for the particle. Perfectly diffusing systems exhibit γ values of 1, particles over and under γ exhibit superdiffusion and subdiffusion, respectively.

Random walk code was implemented, the mean square displacement and alpha coefficients were determined for both individual particles and as an average of all particle trajectories the values of γ approximated a Gaussian distribution with respect to γ while the average was consistent with nearly ideal diffusion. To further emulate our data, each trajectory was assigned a finite probability at each time point to be lost, mimicking a loss in tracking. This provides us with a distribution of particle lifetimes in similar manner to gathered data.

Chapter Two: Goals

Single particle tracking of chromatin of interphase chromatin has previously been studied [39, 45] and has been reported to undergo random confined motion with ATP sensitive jumps. It has also been reported that chromatin dynamics are suppressed in S phase when compared to G1 and G2 phase. While our temporal resolution is limited, data is collected in mass such that we are able to analyze thousands of particle trajectories simultaneously. This provides higher statistical confidence in measurements as well as the ability to analyse multiple populations of chromatin including heterochromatin and euchromatin, as our tracking encompasses the whole of the nucleus. We wish to examine the effect of replication machinery on chromatin dynamics, in particular to explain the diminished mobility in S phase chromatin. Using our particle tracking system, chromatin co-localizing with replication machinery can be compared with non co-localizing particles. We also wish to establish a connection between replication inhibitors on chromatin mobility. Hydroxurea and aphidicolin are two known replication inhibitors which use separate mechanism to cause disruption in S phase. It has been previously established that aphidicolin acts to disassociate the replication machinery from chromatin, whereas hydroxurea leaves the machinery attached but replication is prevented. If chromatin dynamics are modified by replication machinery, we may observe changes in mobility for the hyrdoxurea rather than aphidicolin. The confinement of chromatin to nuclear compartments has been well established, however there is little known about this mechanism. Binding events to an internuclear matrix has been proposed by many groups as the mechanism, however this has not been observed directly.

Chapter Three: Methods and Materials

Cell preparation

The Hela-Kyoto cells, a human cancerous ovarian cell line, were used for all chromatin studies. HeLa cells expressing GFP-PCNA and Cy3-dUTP were imaged using a laser confocal microscope with imaging at 1Hz. Typically GFP-LacI/lacO is used to observe DNA *in vivo*, however Cy3-dUTP was found to increase the foci count and to prevent any preferential binding in different chromatin environments. Images were first separated into their respective channels of chromatin bound to Cy3-dUTP and replication machinery with GFP-PCNA. Images were masked using a custom created function in MATLAB in order to restrict analysis to those particles inside the nucleus. Detection of particles was undertaken through a trou wavelet analysis [47]. While typical studies on chromatin employ the Lac Operator-Repressor, in which a GFP florophore is attached to the Lac OP/Rep which then binds to RNA polyermase binding sites, Cy3-dUTP (deoxyuridine triphosphate) incorporates directly onto the DNA as a florescent nucleotide, and was found to provide more foci locations. Approximately 1 day after labelling nuclei with Cy3-dUTP a Zeiss LSM510 Meta using a 63x 1.4 NA oil immersion objective was used to image the nuclei.

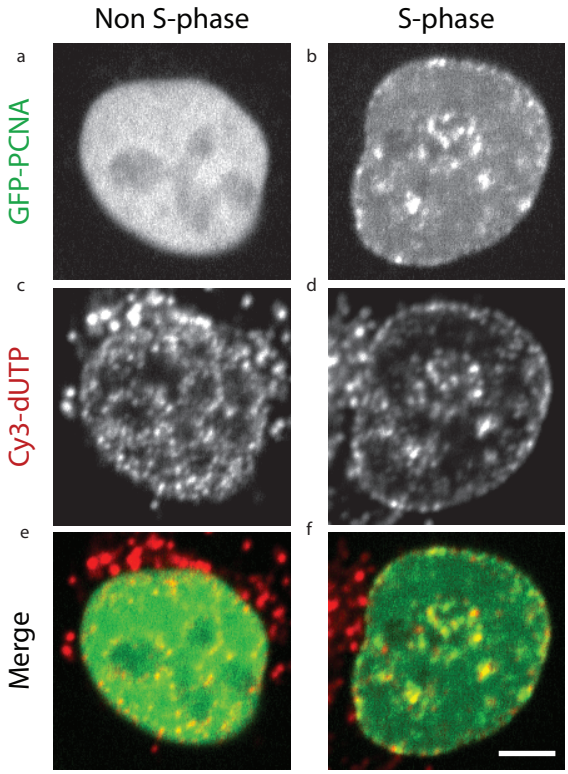

Figure 6: Identification of cell phase

(a-b) Cells are classified as either non S phase or S phase by the punctate nature of the PCNA. (c-d)Cy3-dUTP is incorporated into the nucleus emerging as foci with $\approx$ 230nm diameter. e-f: merge of two channels, replication machinery PCNA co-localize with Cy3-dUTP

The distinctions between cell phases were assigned using the characteristic feature of GFP-PCNA. S phase GFP-PCNA expresses as punctate features throughout the nuclei, where as G1 and G2 exhibit dispersed florescence. Images were taken each second to minimize photobleaching as to contain the florescence through the entirety of interphase.

Detection and Tracking

Nuclei were first segmented using a watershed transformation algorithm to characterize all particle in view as inside our outside the nucleus as to only track chromatin inside the nucleus. This algorithm finds an intensity profile of the images then creates boundaries based upon locations of intensity maxima and minima In order to observe chromatin dynamics *in vivo*, chromatin and replication machinery are first identified by a wavelet based detection algorithm with with a focal size of 100nm [47]. A global optimization tracker described in was used to track all particles within a nucleus simultaneously [48]. The tracking system minimizes the cost associated with connecting particle trajectories. Trajectories with large particle movements are less likely to occur than particles with short trajectories, higher costs are assigned to these and a solution with minimum cost is found. Particle trajectories are collected and fit using equation 11. Each nuclei contributes approximately 50 chromatin sites. For distance dependent effects in S phase, the GPA-PCNA was detected using the described wavelet detection. Each tracked chromatin foci was assigned a nearest neighbour from the PCNA channel as to correlate the effects of replication machinery on chromatin mobility. Colocalization was characterized as chromatin foci and PCNA to be within 50nm.

Calculation of MSD and Jackknife error

The tracking program assigns x and y coordinates to each chromatin foci from each nucleus and culminates the information into a large tracking matrix. We calculate the square displacement for each particle j at each frame i

$$R^2_{j,i} = (x_{j,i} - x_{j,i+1})^2 + (y_{j,i} - y_{j,i+1})^2 \tag{23}$$

The mean square displacement for each particle j at frame i is then

$$MSD_{j,i} = \frac{1}{i}\sum_{n=1}^{i} R^2_{j,n} \tag{24}$$

For most analyses, trajectories of only 50-60 frames are used and averaged to obtain a single MSD.

$$MSD_i = \frac{1}{N}\sum_{j=1}^{N} MSD_{j,i} \tag{25}$$

Where N is the number of trajectories within a given criteria. Variance is calculated amongst the trajectories from the jackknife method where individual trajectories are taken out of the collection of data and its' variance calculated [49]. At each frame i the variance is calculated by

$$\sigma_i^2 = \frac{N-1}{N}\sum_{j=1}^{N}(MSD_{j,i} - MSD_i)^2 \tag{26}$$

Chapter Four: Results

Chromatin motion is Inhibited in S Phase

Trajectories at least 50 frames long were gathered from G1, S, G2, as well as a fixed control. The mean square displacement was calculated using these trajectories with sample sizes of 332, 1,042, 301 and 201 respectively. The results are summarized in the table below. We observe that S phase shows slower movement that both G1 and G2 phase, consistent with previous findings. Our fixed cells undergo what we measure as a slight diffusion coefficient although with the error this can be attributed as negligible. We expect chromatin in fixed cells to undergo virtually no diffusion and this measurement can be attributed to our error result from signal to noise.

Phase	Diffusion Coefficient x10^{-5} μm^2/s	Standard Deviation x10^{-6} μm^2/s
G1	4.77	4.25
S	3.14	1.68
G2	4.47	3.50
Fixed	0.9	0.3

Table 1: Mobility is inhibited in S phase chromatin

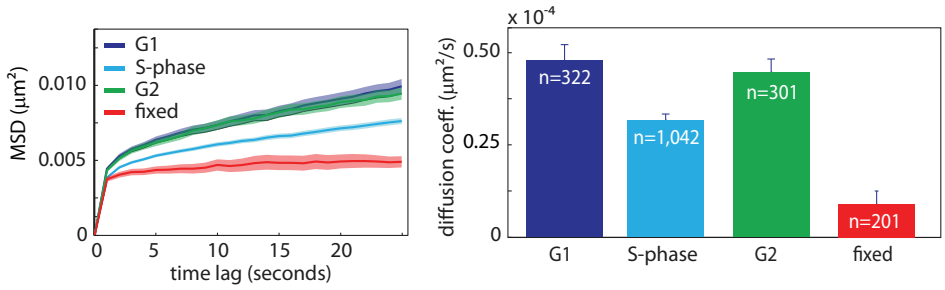

Figure 7: Distribution of diffusion coefficients from interphase.
a) Mean square displacement through interphase and fixed cells. b) Diffusion coefficients calculated from a), G1 and G2 exhibit coefficients of 4.775x10^{-5} μm^2/s and 4.475x10^{-5} μm^2/s whereas S exhibits diffusion at a rate of 3.145x10^{-5} μm^2/s. Fixed cells exhibit minimal diffusion at 9x10^{-6} μm^2/s

Motion with Co-localizing Replication Machinery

With the decrease in mobility in S phase established, distance dependent effects by proximity to GFP-PCNA was carried out in all phases, using a proximity of 1 pixel 50nm between GFP-PCNA and Cy3-dUTP foci to describe co-localizing particles. Non S phase nuclei (G1 and G2) were binned together. Trajectories matching the minimum lengths described above were binned into locations of proximity to nearest replication site. Previous work showed steadily increasing diffusion coefficients in S phase to a maximum value when replication machinery was far enough away from a chromatin foci. We estimate the use of a maximum distance of 1 pixel 1nm for co-localizing particles into two bins : from 0 to 50nm and everything greater than 50nm. Non S phase chromatin showed diffusion coefficients for the co-localizing and non-co localizing bins as (4.15 $\pm$ 0.35)x10^{-5} μm^2/s and (4.10 $\pm$ 0.425)x10^{-5} μm^2/s respectively. As the distributions are approximately Gaussian, a t-test was carried out between these two bins and a p value of 0.3699 was calculated for the two bins. We next examined mobility in S phase using the same criteria as described above. Mobilities of (2.475 $\pm$ 0.19)x10^{-5}

μm^2/s and 2.95 $\pm$ 0.14)x10^{-5} μm^2/s were found for the two bins indicating a machinery dependent effect of mobility. While we observe a distance dependent relationship in S phase, the mobility of non co localizing particles has not yet regained that of non S phase chromatin.

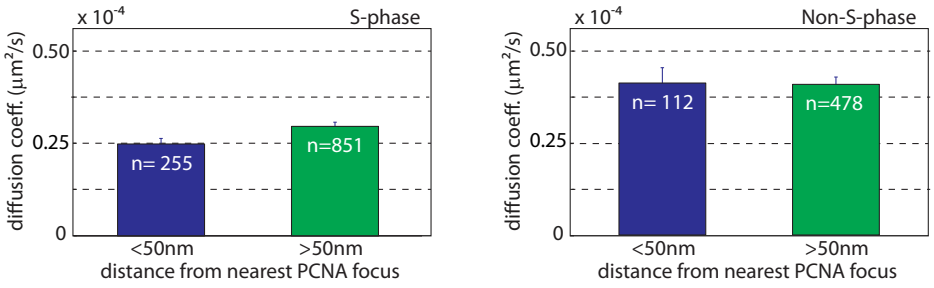

Figure 8: Mobility as function of PCNA distance
a)S phase mobility as a function distance from PCNA foci; Co-localizing Cy3-dUTP and GFP-PCNA exhibit diminished mobility. b) Non S phase chromatin mobility shows no dependence on distance to replication GFP-PCNA.

Drug Treatments on Chromatin Motion

We next wanted to examine the effects of known replication inhibitors aphidicolin and hydroxurea on chromatin dynamics to support the hypothesis of replication machinery's role in chromatin mobility repression. It has been established that aphidicolin disassociates replication machinery from the replication fork, and hydroxurea inhibits replication whilst leaving the machinery attached to DNA. Binning in the same manner as described above we observed aphidicolin with diffusion coefficients for the 0 to 50nm bin and everything greater than 50 nm as (2.225 $\pm$ 0.10)x10^{-5} μm^2/s and 2.600 $\pm$ 0.21)x10^{-5} μm^2/s. As we would expect the difference between these two to be minimal, the difference can be seen in Hydroxurea which exhibits diffusion coefficients in the bins as (2.125$\pm$0.21)x10^{-5} μm^2/s and (2.90$\pm$0.27)x10^{-5} μm^2/s.

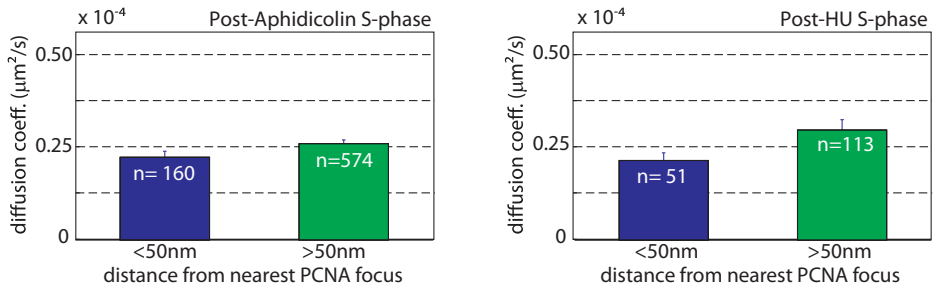

Figure 9: Drug treatments effect on chromatin mobility
a) Post treatment with aphidicolin show a small deviation between co-localizing and non co-localizing replication machinery. b) After treatment with hydroxurea there is a greater effect from proximity to replication machinery.

Euchromatin and Heterocrhomatin

The nucleus is compartmentalized in a similar manner to the cell as a whole. Heterochromatin and euchromatin occupy the periphery and interior of the nucleus respectively. They are also different in compaction and their transcriptional activity. As we observe chromatin foci scattered along the nucleus we are able to sample from both of these populations. Heterochromatin is associated with the nuclear lamina and as such only occupies the first 100nm of the nucleus whereas eurchromatin is located to within the nucleus. We locate each focus proximity to the nuclear periphery by way of our initial mask of the nucleus and bin foci from 0 to 100nm to the periphery and all other foci distances. We find that in non S phase foci nearest to the cell periphery exhibit diffusion rates as (4.175$\pm$0.57) x10^{-5} μm^2/s whereas in the nuclear interior rates are (4.75$\pm$0.30)x10^{-5} μm^2/s. Moving to S phase the behavior is modified, yielding diffusion coefficients from the border to the interior as (3.525$\pm$ 0.42)10^{-5} μm^2/s and (3.125$\pm$ 0.17)x10^{-5} μm^2/s.

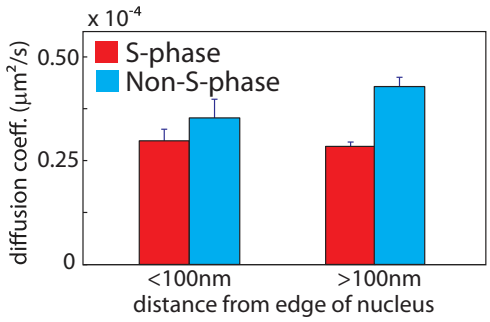

Figure 10: Mobility as a function of distance to nuclear periphery
Heterochromatin, located within ≈ 100nm of the nuclear periphery and euchromatin show higher mobility in S phase; the affect is seen to be more pronounced in euchromatin.

Diffusion properties

Characterizing the specific type of motion can lead to biological significance, in Kv 2.1 channels, sub-diffusion caused by a non-ergodic continuous time random walk (CTRW) was shown to arise from transient binding events to membrane [50]. We first characterized the motion by performing ergodicity measurements between the time and ensemble averages. The time ensemble average calculates the average displacement of each trajectory

$$< R^2 >_{temp} = \frac{1}{T}\sum_{i}^{T} R_{i,j}^2 \tag{27}$$

$$< R >_{temp} = \left(\frac{1}{T}\sum_{i}^{T} R_{i,j}^2\right)^{\frac{1}{2}} \tag{28}$$

Whereas the ensemble average calculates the average frame to frame displacement of all trajectories

$$< R^2 >_{ens} = \frac{1}{N}\sum_{j}^{N} R_{i,j}^2 \tag{29}$$

$$< R >_{ens} = \left(\frac{1}{N}\sum_{j}^{N} R_{i,j}^2\right)^{\frac{1}{2}} \tag{30}$$

Performing these measurements on our random walk simulation with typical time lengths and trajectories shows produces similar time and ensemble averages.

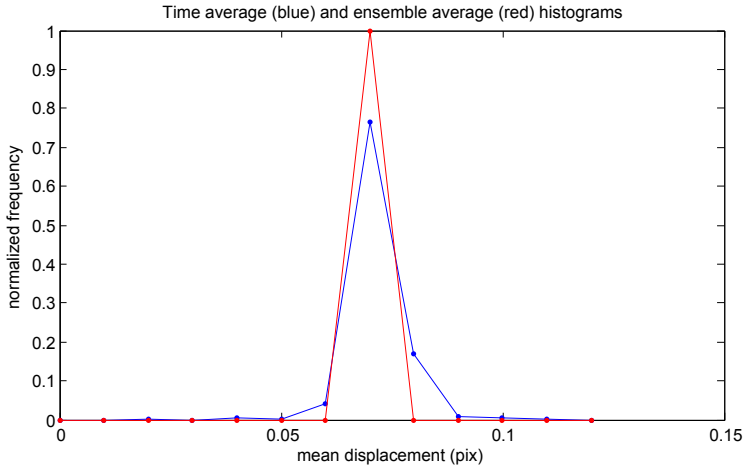

Figure 11: Ergodicity is conserved in a perfect random walk $< R >_{ens} = < R >_{temp}$ for conserved ergodicity. In the random walk simulation of 1000 trajectories with 120 time steps, both the temporal and ensemble average of the displacement reach the same distribution.

Performing these measurements on our fixed cells produces the following

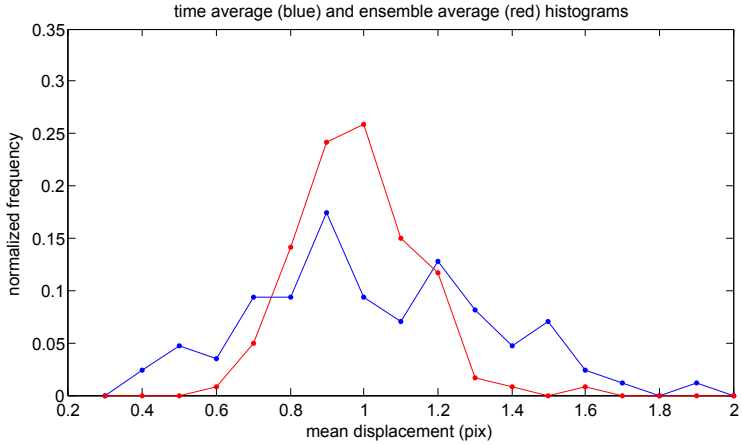

Figure 12: Ergodicity in Fixed Cells

The temporal and ensemble averages for fixed cells approach similar distributions; with 400 particles at 120 frames.

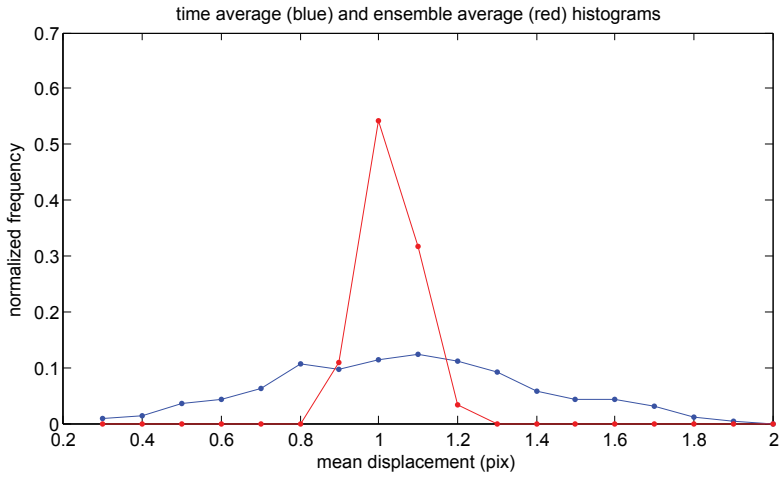

Figure 13: Ergodicity in S Phase

The temporal average diverges from the expected sharpness from the simulation, while N_{ens} constitutes 120 data points, N_{temp} is composed of 2128 data points.

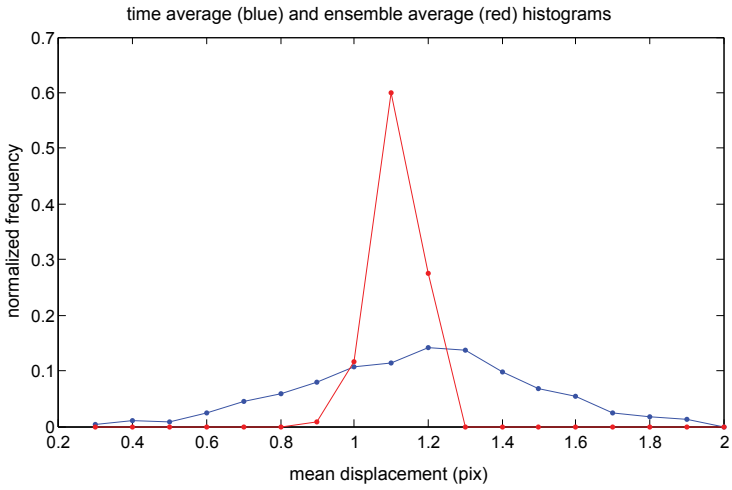

Figure 14: Ergodicity in Non S Phase
The ensemble average approaches a Gaussian similar to the simulation while the temporal average again deviates. N_{ens} is again 120 data points and N_{temp} is composed of 1589 data points

The diffusional properties vary between particles, specifically for given lifetimes particles exhibit altered diffusion rates. In simulations of perfect random walk, unless an inherent heterogeneity is constructed within each particle, diffusional rates are independent of lifetime.

When we observe the displacement of living nuclei, noting that 1pixel=50nm

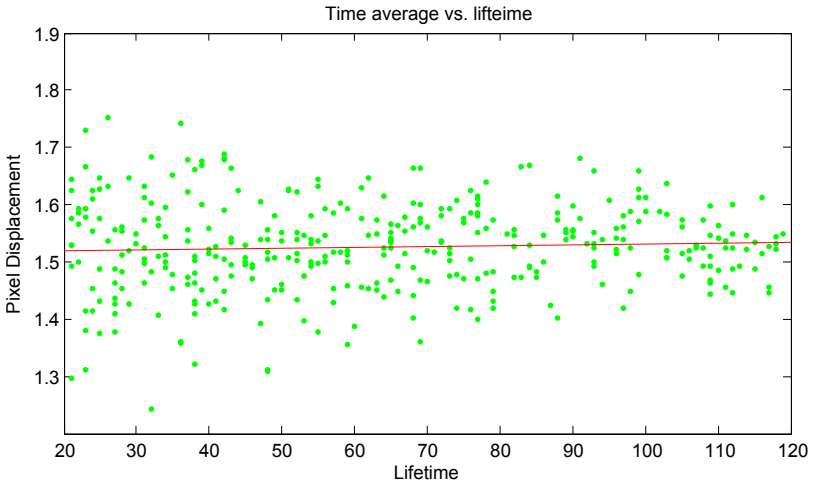

Figure 15: Sim Lifetime VS. Displacement
Displacement of a simulation particle is independent of lifetime

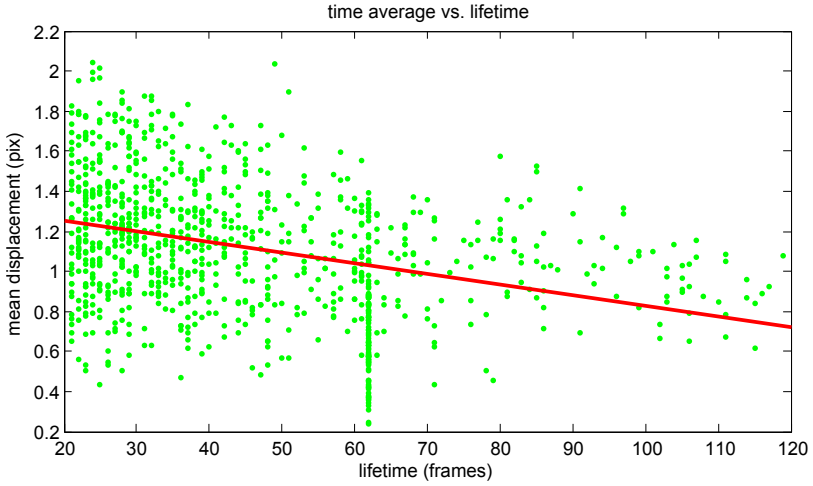

Figure 16: S Phase Lifetime vs. Displacement
Average particle displacements show dependence on the lifetime of the chromatin foci using N=1000, t=120s.

The line of mean trajectory displacements at 62 seconds results from a list of movies which all end at 62 seconds, however the distribution of particles lie below the least squares line and if the movies were extended the points would spread out below. Intuitively this agrees with the tracking; slow moving particles are more likely to be tracked longer than their faster moving counterparts, which either move out of the image plane

or are unable to tracked due to gap closing issues as described previously.

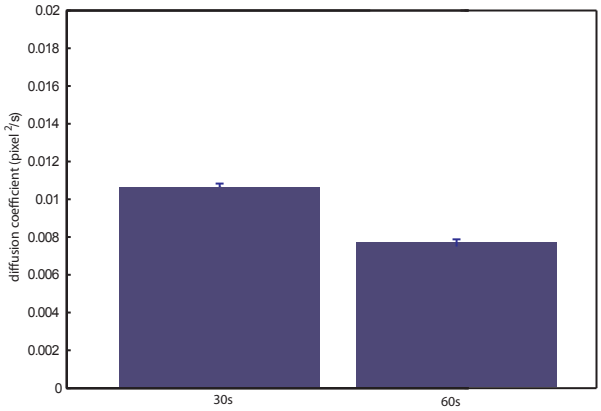

Figure 17: Mobility and Lifetime
Diffusion coefficients of particles with 30s and 60s lifetimes. The ability to track particles for extended periods of time is invariable tied into their mobility due to tracking errors or travelling out of the focal plane.

We next looked to characterize the shape of the mean square displacement by assuming the mean square displacement will scale as a power law we can use the mobility power, γ as an indication for the diffusion type. Ideal random motion yields a γ of 1 and the MSD goes linearly in time.

$$< x^2 > \propto At^{\gamma} \tag{31}$$

Foci scaling as $\gamma > 1$ are deemed super-diffusive as they seem to travel in 1 direction preferentially until the limit when there distance from a starting point is proportional to their velocity and time which is deemed as a ballistic trajectory. Subdiffusion then occurs opposite of these situations when $\gamma < 1$.

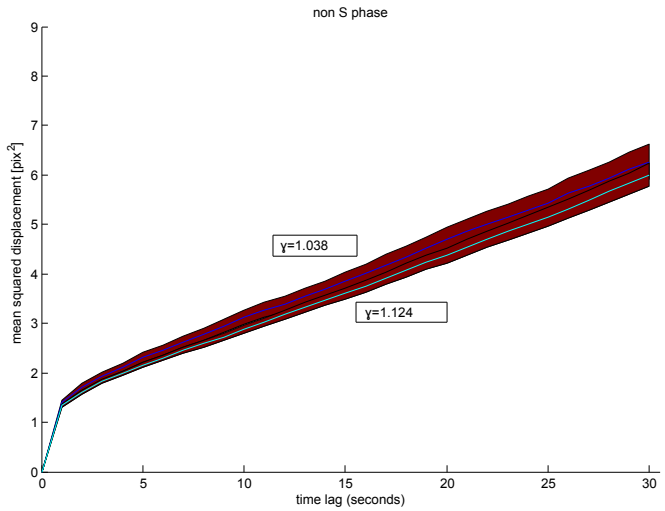

Figure 18: Non S phase Diffusion
Non S phase MSD exhibits close to perfect diffusion with coefficients 1.03 and 1.12, where the MSD grows linearly with time. The two lines correspond to our binning critera of proximity to replication machinery.

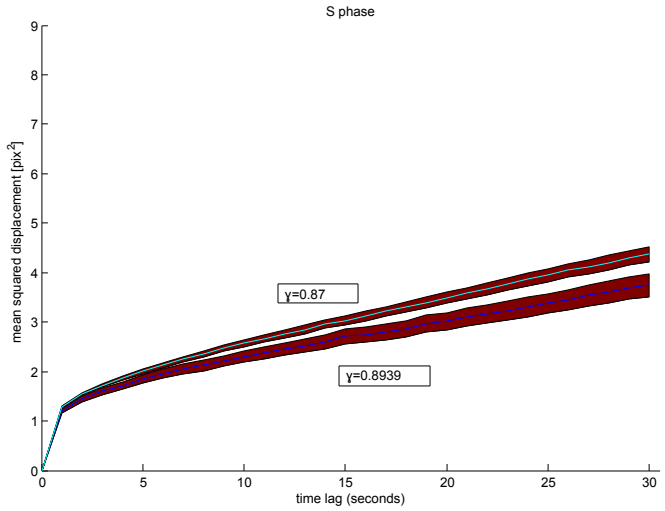

Figure 19: S phase Diffusion

S phase MSD shows gamma coefficients of 0.87 and 0.89 The lower curve represents trajectories within 50nm to replication machinery and the teal curve everything greater than 50nm away from replication machinery.

Non uniformity on a circle

To explore the idea of individual trajectories undergoing active transport, we can define the direction which they travel on a circle at angle θ from the origin. Particles undergoing random motion will explore all space/angles in their proximity whereas a particle under an active transport system (be it biological or drift) will prefer one direction over the rest. We can test for statistical significance by employing circular uniformity and by the use of the Hodges-Anje test

$$p = \frac{(n-2)\binom{n}{m}}{2^{n-1}} \tag{32}$$

$$= \frac{(n-2m)\frac{n!}{m!(n-m)!}}{2^{n-1}} \tag{33}$$

We can make the approximation if n, the number of points, is greater than 50

$$p \approx \frac{\sqrt{2\pi}}{A} exp\left[\frac{-\pi^2}{8A^2}\right] \tag{34}$$

Where A is

$$A = \frac{\pi\sqrt{n}}{2(n-2m)} \tag{35}$$

And m is the test statistic dependent on the sample size relating to the smallest amount of data under the null hypothesis that can be placed on the edge of a circle.

We first want to observe the behavior on our random walk simulation, while there is no anisotropy particles can be expected to traverse preferentially based on a limited time frame. Choosing particle trajectories that are at least 50 frames long to a maximum of 120 frames we compute the Hodges-Anje test to either accept the null hypothesis H0 that the points are evenly distributed around the circle or the alternative hypothesis HA

that there is a non uniform distribution around the circle at the 95% confidence level [51]

.

Table 2: Hodges-Anje Test

Dataset	N	# HA	% HA
Random Simulation	2035	81	0.0398
Non S Phase	1589	15	0.0094
S Phase	2128	0	0
Fixed	411	1	0.0024

Trajectories which pass the null hypothesis

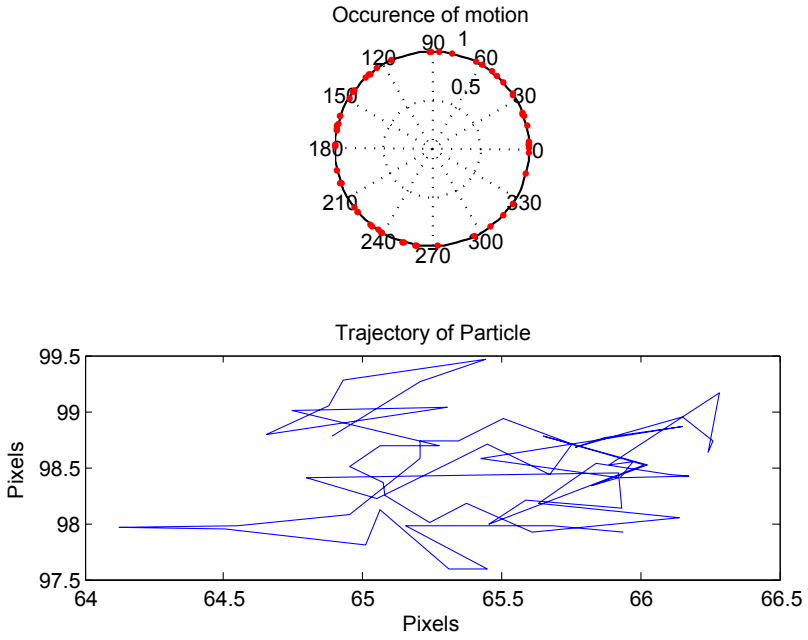

Figure 20: Pass of the null hypothesis
A particle shows no anisotropy by travelling in all directions equally

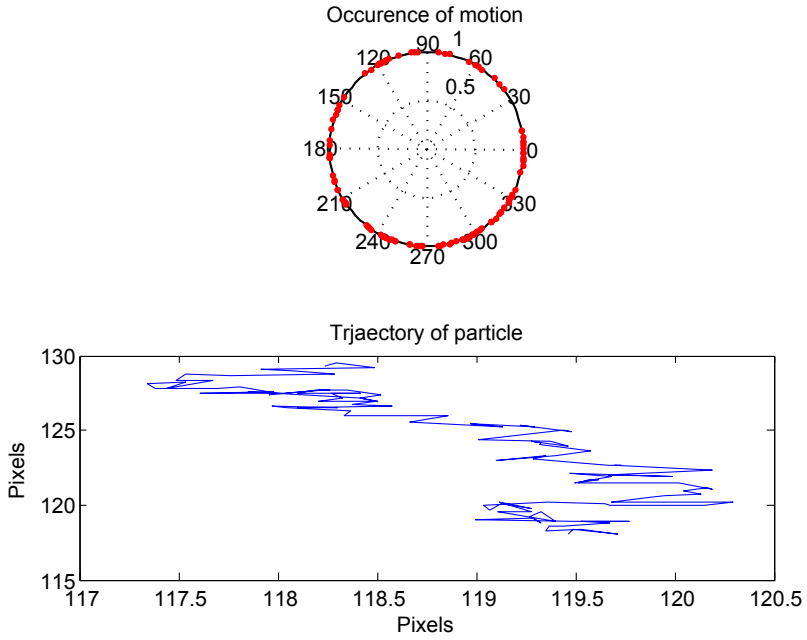

Figure 21: Failure of the null hypothesis
A particle seems to travel toward one direction more often than others.

Chapter Five: Discussion

We have applied quantitative methods in image analysis to analyse the motion of chromatin in interphase. Previous studies have reported inhibited motion in S phase, and here we set out to quantify that effect through the behavior of replication machinery. Non S phases reported mobilities at 4.775x10^{-5} μm^2/s and 4.475x10^{-5} μm^2/s respectively whereas S showed significantly inhibited mobility at 3.175x10^{-5} μm^2/s. We hypothesized that S phase mobility is resultant from active replication. For this we employed a dual channel assay with GFP-PCNA. Establishing a criteria of replication between chromatin sites and GFP-PCNA foci as a maximum of 100nm, we label sites as actively replicating or quiescent. We observed changes in mobility between these two bins as 2.475x10^{-5} μm^2/s and 2.95x10^{-5} μm^2/s. We expect mobility in the 2nd bin to at least approach the global value of 3.175x10^{-5} μm^2/s. The deviation in this can most likely be explained by under-sampling trajectories under replication. Even with under-sampling, the deviation from Non-S chromatin mobility and inactive S chromatin is still likely subject to other influencing forces. When characterizing the diffusional characteristics we found non S phase exhibits normal to slightly superdiffusive behavior whereas non S shows tendencies towards subdiffusion. This subdiffusion may be resultant of an additional biological process in S phase to suppress chromatin motion.

We observe that the system, regardless of phase tends towards a non-ergodic random walk when compared to ergodic confined random walk simulations [50] hinting at memory effects associated with chromatin mobility. We expect a perfect random walk such as our simulation to yield a value of 1. Sub-diffusion in S phase indeed may be resultant of biological forcing. Since this diffusional behavior occurs for both non co-localizing and co-localizing PCNA foci. It has been reported that chromatin under-

goes linear motion, dependent on ATP levels. We incorporated statistical analysis with random random distributions on a circle in attempts to isolate trajectories which travel preferentially in one direction through the Hodges-Anje probability testing. This work however, we see no evidence of this phenomenon; this can most likely be attributed to our slower time resolution as it has been reported that these jumps are on the order of 0.3-2 seconds. While we have been able to explain the decrease in mobility in S phase chromatin through co-localization with replication machinery, the global reduction in mobility hints at another process, likely binding events in the nuclear cytosol.

References

[1] K. E. V. Holde, *Principles of Physical Biochemistry*. Pearson Prentice Hall, 1998.

[2] B. Alberts, A. Johnson, J. Lewis, M. Raff, K. Roberts, and P. Watler, *Molecular Biology of the Cell*. Garland Science, 2008.

[3] G. M. Cooper, *The Cell*. Sinauer Associates, 2000.

[4] J. Watson and F. Crick, "A structure for deoxyribose nucleic acid," *Nautre*, 1953.

[5] N. A. Campbell and J. B. Reece, *Biology Concept and Connections*. California, 1997.

[6] M. Ball, "Dna chemical structure." http://upload.wikimedia.org/wikipedia/commons/e/e4/DNA_chemical_structure.svg , March 2007. Accessed: 6/20/2012.

[7] A. Olins and D. Olins, "Visualization of chroamtin substructure," *J. Cell Biology*, 1975.

[8] R. D. Kornberg, "Chromatin strucutre: A repeating unit of histones and dna," *Science*, 1974.

[9] V. Bakayev and A. Melnikov, "Studies on chromatin. ii. isolation and characterization of chromatin subunits," *Nucleic Acids Res*, 1975.

[10] J. T. Finch, L. C. Lutter, D. Rhodes, R. S. Brown, B. Rushton, M. Levitt, and A. Klug, "Structure of nucleosome core particles of chromatin," *Nature*, 1977.

[11] G. Arents, R. W. Burlingame, B.-C. Wang, W. E. Love, and E. N. Moudriankis, "The nucleosomal core histone octamer at 3.1 a resolution: a tripartite protein assembly and a left-handed superhelix," *Proc. Nati. Acad. Sci.*, 1991.

[12] J. M. Harp, B. L. Hanson, and G. J. Bunick, *The core particle of the nucleosome*, ch. 2. Elsevier, 2004.

[13] M. Elstov, K. Maclellan, K. Frangakis, and K. Maeshima, "Analysis of cryo-electron microscopy images does not support the existence of 30-nm chromatin fibers in mitotic chromomes in situ," *Proc Natl Acad Sci*, 2008.

[14] R. Schneider and R. Grosscdhel, "Dynamics and interplay of nuclear architecture, genome organization, and gene expression," *Genes Dev*, 2007.

[15] D. Leja, "Chromatin." www.genome.gov . Accessed:6/13/2012.

[16] M. Hubner and D. Spector, "Chromatin dynamics," *Annual Review of Biophysics*, 2010.

[17] A. Errico and V. Costanzo, "Differences in the dna replication of unicellular eukaryotes and metazonas: known unknowns," *EMBO reports*, 2010.

[18] J. Sun and D. Kong, "Dna replication origins, orc/dna interaction, and assembly of re-replication complex in eukaryotes," *Acta Biochim Biophys Sin*, 2010.

[19] H. Leonhardt, H.-P. Rahn, P. Weinzierl, A. Sporbert, T. Cremer, D. Zink, and M. C. Cardoso, "Dynamics of dna replication factories in living cells," *Journal of Cell Biology*, 2000.

[20] B. Alberts, A. Johnson, J. Lewis, M. Raff, K. Roberts, and P. Watler, *Molecular Biology of the Cell*. Garland Science, 2008. Figure 5-19.

[21] S. Gorisch, A. Sporbert, J. Stear, I. Grunewald, D. Nowak, E. Warbrick, H. Leonhardt, and M. Cardoso, "Uncoupling the replication machinery: replication fork progression in the absence of processive dna synthesis," *Cell Cycle*, 2008.

[22] R. Wheeler, "Cell cycle." http://upload.wikimedia.org/wikipedia/commons/d/d0/Cell_Cycle_2.svg , 2006. Accessed: 7/10/2012.

[23] A. Groth, W. Rocha, A. Verreault, and G. Almouzni, "Chromatin challengers during dna replication and repair," *Cell*, 209.

[24] V. Jackson, "Deposition of newly synthesized histones: hybrid nucleosomes are not tandemly arranged on daughter dna strands," *Biochemistry*, 1988.

[25] J. Sogo, H. Stahl, T. Koller, and R. Knippers, "Structure of replication simian virus 40 minichromosomes. the replication fork, core histone segregation and terminal structures," *Journal of Molecular Biology*, 1986.

[26] A. Ehrenhofer-Murray, "Chromatin dynamics at dna replication, transcription and repair," *European Journal of Biochemistry*, 2004.

[27] M. Nakao, "Epigenetics: interaction of dna methylation and chromatin," *Gene*, 2001.

[28] A. McNairn and D. Gilbert, "Epigenomic replication: linking epigenetics to dna replication," *Bioessays*, 2003.

[29] H. Qian, M. Sheetz, and E. Elson, "Single particle tracking," *Biophysical Journal*, 1991.

[30] D. Loerke, M. Mettlen, D. Yarar, K. Jaqaman, H. Jaqaman, G. Danuser1, and S. L. Schmid, "Cargo and dynamin regulate clathrin-coated pit maturation," *PLoS Biology*, 2009.

[31] "Brownian motion and the langevin equation." http://units.physics.uwa.edu.au/__data/page/115450/lecture3_(brownian_motion)-NF.pdf , September 2005. Accessed:5/10/2012.

[32] "Langevin equation." http://xbeams.chem.yale.edu/~batista/vaa/node59.html.

[33] W. Coffey, Y. Kalmykov, and J. Waldron, *The Langevin Equation*.

[34] T. Cremer, P. Lichter, J. Borden, D. Ward, and L. Manuelidis, "Chromsome territories-a functional nuclear landscape," *Current Opinion Cellular Biology*, 2006.

[35] W. Marshall, "Order and disorder in the nucleus," *Curr. Biol*, 2002.

[36] A. Pliss, K. Malyavantham, S. Bhattacharya, M. Zeitz, and R. Berezney, "Chromosoma," 2009.

[37] E. Soutoglouff and T. Misteli, "Mobility and immobility of chromatin in transcription and genome stability," *Current Opinion in Genetics and Development*, 2007.

[38] H. Bornfleth, P. Edelmann, D. Zink, T. Cremer, and C. Cremer, "Quantitative motion analysis of subchromosomal foci in living cells using four-dimensional microscopy," *Biophysical Journal*, 1999.

[39] V. Levi, Q. Ruan, M. Plutz, A. S. Belmont, and E. Gratton, "Chromatin dynamics in interphase cells revealed by tracking in a two-photon excitation microscope," *Biophysical Journal*, 2005.

[40] M. Saxton and K. Jacobson, "Single particle tracking: Applications to membrane dynamics," *Annual Review of Biophysics*, 1997.

[41] J. Bridger, S. Boyle, I. Kill, and W. Bickmore, "Re-modelling of nuclear architecture in quiescent and senescent human fibroblasts," *Current Biology*, 2000.

[42] J. Walter, L. Schermelleh, M. Cremer, S. Tashiro, and T. Cremer, "Chromosome order in hela cells changes during mitosis and early g1, but is stably maintained during subsequent interphase stages," *Journal of Cell Biology*, 2003.

[43] T. Tumbar and A. Belmont, "Interphase movements of a dna chromosome region modulated by vp16 transcriptional activator," *Nat. Cell Biol.*, 2001.

[44] M. Bronco and A. Pombo, "Intermingling of chromosome territories in interphase suggests role in translocations and transcription-dependent associations," *PLoS Biology*, vol. 4, no. e138, p. 10.1371/journal.pbio.0040138, 2006.

[45] S. M. Gasser, "Visualizing chromatin dynamics in interphase nuclei," *Science's Compass*, 2002.

[46] *Statistical Mechanics*. Elsevier, 2008.

[47] J. Olivo-Marin, "Extraction of spots in biological images using multiscale products," *Pattern Recognition*, vol. 35, pp. 1989–1996, 2002.

[48] K. Jaqaman1, D. Loerke, M. Mettlen, H. Kuwata, S. Grinstein, S. Schmid, and G. Danuser, "Robust single-particle tracking in live-cell time-lapse sequences," *Nature Methods*, 2008.

[49] E. Bradley, *The Jackknife, the Bootstrap and Other Resampling Plans*. Society for Industrial and Applied Mathematics, 1982.

[50] A. Weigel, B. Simon, M. Tamkum, and D. Krapf, "Ergodic and nonergodic processes coexist in the plasma membrane as observed by single-molecule tracking," *Proceedings of the National Academy of Sciences*, 2011.

[51] J. Zar, *Biostatistical Analysis*. Prentice Hall, 2010.

Appendix

Table 3: Interphase behavior

Name	Diffusion Coefficient x10^{-5} $\frac{\mu m^2}{2}$	Std Dev x10^{-6} $\frac{\mu m^2}{s}$	Sample Size
G1	4.775	4.250	322
S	3.175	1.688	1041
G2	4.475	3.500	301
Fixed	0.90	3.500	201
Non S 0-50nm	4.15	4.250	112
Non S $>$ 50nm	4.100	1.986	478
S 0-50nm	2.4750	1.485	255
S $>$ 50nm	2.950	1.1073	851